Annals of Nuclear Energy 112 (2018) 109–119

Contents lists available at ScienceDirect

Annals of Nuclear Energy

journal homepage: www.elsevier.com/locate/anucene

Effect of axial power distribution on flow instability in parallel channels with water at supercritical pressures

Edward Shitsi *, Seth Kofi Debrah, Vincent Yao Agbodemegbe, Emmanuel Ampomah-Amoako

Department of Nuclear Engineering, School of Nuclear and Allied Sciences, University of Ghana, P.O. Box AE 1, Atomic Energy, Kwabenya, Accra, Ghana

ARTICLE INFO

Article history:
Received 26 February 2017
Received in revised form 19 September 2017
Accepted 1 October 2017
Available online 9 October 2017

Keywords:
Numerical investigation
Supercritical pressure
Flow instability
Axial power shape
Pseudo-critical region
Parallel channel

ABSTRACT

Stability of the operation of SCWR at the supercritical conditions has become a major concern to the nuclear engineers worldwide, especially around the pseudo-critical point where dramatic changes of the fluid properties are experienced. This concern of addressing supercritical flow instability is due to various studies showing that the efficiency of light water reactors can be improved considerably from 33% at subcritical pressures to 45% at supercritical pressures.

This work investigates effect of axial power distribution on flow instability in parallel channels with water at supercritical pressures. The axial power distributions considered include axially decreased and homogeneous axial power shapes. The study also seeks to examine the performance of the 3D numerical tool STAR-CCM+ in predicting flow instability at supercritical pressures. The effects of parameters such as mass flow rate, pressure and gravity on flow instability were also discussed. Sensitivity analysis of some selected turbulence models and time steps were initially carried out with the aim of selecting suitable turbulence model and time step for the numerical simulations. For a system operated exclusively at two different pressures 23 MPa and 25 MPa with 125 kg/h mass flow rate, inlet temperatures from 180 °C to 360 °C and with gravity influence, stability of the system with axially decreased or homogeneous power shape decreases and increases respectively below and above a particular threshold power with inlet temperature. The system was found more stable with homogeneous Axial Power Shape (HAPS) than that of axially decreased power shape (ADPS). Similar observation was made for a system operated at mass flow rate of 125 kg/h, system pressure of 23 MPa, and with or without gravity influence. When the system is operated at 23 MPa pressure, 145 kg/h mass flow rate and with gravity influence, there is a threshold power below which stability decreases and above which stability increases with inlet temperature for HAPS. In this case, there is no inflection point for ADPS and the stability deceases with inlet temperature. At low inlet temperatures, the system is more stable with ADPS but at high inlet temperatures the system is more stable with HAPS for the system operated at 23 MPa pressure and 145 kg/h mass flow rate. The system with ADPS or HAPS becomes more stable with the change of the system operated with gravity influence to the system operated without gravity influence, and also with the change of system pressure from 23 MPa to 25 MPa. With the change of the system mass flow rate from 125 kg/h to 145vkg/h, the system with ADPS becomes more stable at low inlet temperatures and less stable at high inlet temperatures, whereas the system with HAPS becomes less stable for the various inlet temperatures. For a system operated under experimental conditions of 125 kg/h mass flow rate, 23 MPa pressure, inlet temperatures from 180 °C to 260 °C and with gravity influence, the trends of the numerical instability boundary results agree quite well with the trends of the experimental instability boundary results for most of the inlet temperatures, but there is no inflection point for experimental HAPS as it is the case for numerical HAPS. The system with HAPS is more stable than that with ADPS, a finding also obtained for the experimental results. The dynamics characteristics such as amplitude and period were also compared with experimental results for ADPS at mass flow rate of 125 kg/h, 23 MPa, and with gravity influence. The experimental amplitude was largely under-predicted and the experimental period was quite well predicted by the numerical tool adopted. The results of this study show that the type of axial power shape

Abbreviations: ADPS, axially decreased power shape/distribution; BWR, boiling water reactor; DWOs, density wave oscillations; HAPS, homogeneous axial power shape/distribution; LWRs, light water reactors; MSBs, marginal stability boundaries; NPIC, Nuclear Power Institute of China; PWR, pressurized water reactor; SCWR, supercritical water-cooled reactor; THRUST, thermal-hydraulic solver undertaking supercritical water.

* Corresponding author at: Department of Nuclear Engineering, School of Nuclear and Allied Sciences, University of Ghana, P.O. Box AE 1, Atomic Energy, Kwabenya, Accra, Ghana.

E-mail addresses: edwardshitsi@yahoo.com (E. Shitsi), s.debrah@gaecgh.org (S.K. Debrah), vincevalt@gmail.com (V.Y. Agbodemegbe), emmagaec@gmail.com (E. Ampomah-Amoako).

https://doi.org/10.1016/j.anucene.2017.10.003
0306-4549/

adopted in supplying heat to the fluid flowing through heat transfer system has significant effect on the stability of the system. From the comparison of the numerical and experimental results, the 3D numerical tool, STAR-CCM+ code could predict flow instability in the parallel channels irrespective of the type of axial power shape adopted. However, there is an evidence that the presence of heating structures in the geometrical model adopted may change the predicted behavior, as shown in previous works. More relevant experiments at supercritical pressures should be carried out for validation of numerical tools adopted for similar studies.

Nomenclature

$C_{1\varepsilon}$, $C_{2\varepsilon}$, $C_{3\varepsilon}$	turbulence model coefficients
G	acceleration due gravity (m/s^2)
G	mass flux (kg/m^2 s)
G_b	generation of turbulence kinetic energy due to buoyancy (kg J/m^3 s)
G_k	generation of turbulence kinetic energy due to mean velocity gradient (kg J/m^3 s)
G_ω	generation of ω (kg/m s^4)
K	hydraulic loss coefficient
K_{in}	localized pressure drop coefficient at the channel inlet
K_{out}	localized pressure drop coefficient at the channel outlet
L	length of the pipe (m)
L_H	heated length (m)
M_t	total mass flow rate (kg/s)
M_{in1}	total mass flow rate at channel 1 inlet
M_{in2}	total mass flow rate at channel 2 inlet
S_k	source term in k equation (kg J/m^3 s)
S_T	source term in energy equation (kg K/m^3 s)
S_u	source term in x momentum equation (kg/m^2 s^2)
S_v	source term in y momentum equation (kg/m^2 s^2)
S_w	source term in z momentum equation (kg/m^2 s^2)
S_ε	source term in ε equation (kg/m s^4)
S_ω	source term in ω equation (kg/m s^4)
T	emperature (K)
u	velocity (m/s)

Greek letters

ε	turbulent dissipation rate (m^2/s^3)
ω	specific turbulent dissipation rate (1/s)
λ	thermal conductivity (W/m K)
k	turbulent kinetic energy, m^2/s^2
μ	viscosity (Pas)
μ_t	turbulent viscosity (Pas)
ρ	density of the fluid (kg/m^3)
σ_k	Prandtl number correspond to k
σ_ε	Prandtl number correspond to ε
σ_ω	Prandtl number correspond to ω
τ_k	effective diffusivity of k (kg/m s)
τ_ω	effective diffusivity of ω (kg/m s)

Subscripts

b	bulk
g	gravity
In	inlet
out	outlet
p	constant pressure
pc	pseudo-critical

1. Introduction

Stability of the operation of SCWR at supercritical conditions has become a major concern to the nuclear engineers worldwide, especially around the pseudo-critical point where dramatic change of the fluid properties is experienced as shown in Figs. 1–4 (Xi et al., 2014a). This is due to various studies showing that the utilization of supercritical fluids can considerably increase efficiency of light water reactors from 33% at subcritical pressures to 45%. Instability is undesirable as high amplitude sustained flow oscillations beyond uncontrollable limits may cause forced mechanical vibration of components; and also disturb control systems and cause operational problems in nuclear reactors (Ampomah-Amoako, 2013; Nayak and Vijayan, 2008).

There are three kinds of approaches for flow instability investigation including theoretical analysis with frequency domain method (FDM); time domain method (TDM) with one dimensional (1D) and three dimensional (3D) codes; and by experiment. Due to the limitation of high temperature and pressure, there are just few experiments of interest relating to flow instability at supercritical pressures. Most of the investigations are based on FDM and TDM (Xi et al., 2014a). Frequency-domain analysis is based on the linearization of nonlinear equations by perturbing the governing equations around a steady-state point. Once the linear model has been converted from time domain to a frequency domain, exact analytical solutions can be obtained. As a result, marginal stability boundaries (MSBs) in a parameter space can be determined and the space is divided into stable and unstable regions. In order to obtain stability boundaries in Time-domain analysis, the nonlinear time domain approach relies on a digital numerical simulation of

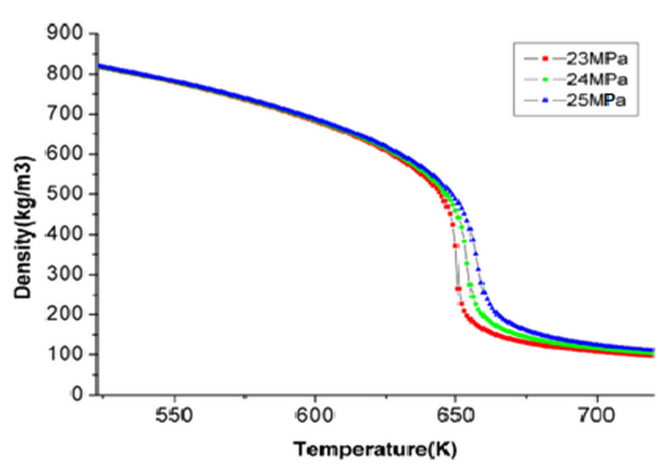

Fig. 1. Density change of water with the increase of temperature.

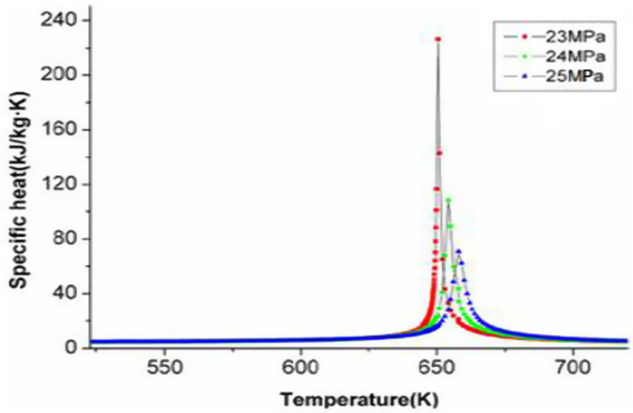

Fig. 2. Specific heat change of water with the increase of temperature.

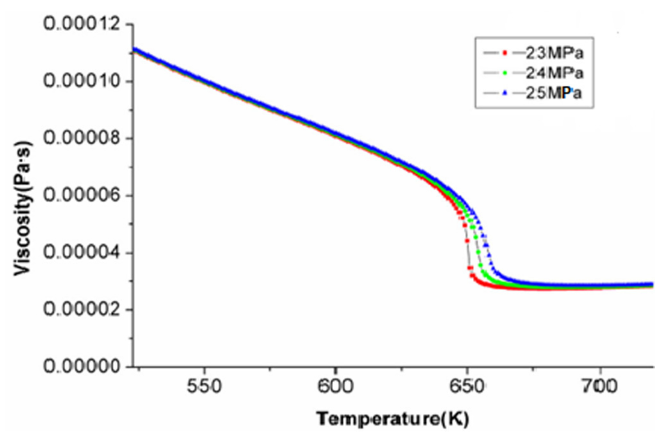

Fig. 3. Viscosity change of water with the increase of temperature.

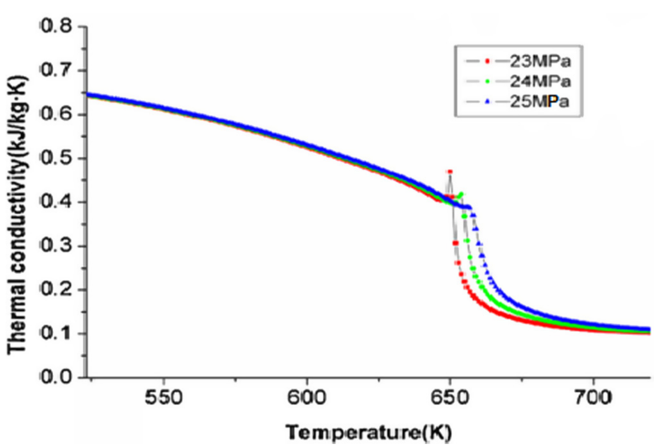

Fig. 4. Thermal conductivity change of water with the increase of temperature.

nonlinear partial differential equations (PDEs) by means of finite-difference techniques (Dutta and Doshi, 2008).

Chatoorgoon (2008) found out that supercritical flow instability in horizontal channels is driven primarily by the state property variation of density with enthalpy; and in particular, the second derivative of density with enthalpy is a dominant term for the onset of flow oscillations in horizontal flow. Sharma et al. (2010) developed a computer linear stability code SUCLIN and used it to perform linear stability analysis of a supercritical water natural circulation loop. The effects of diameter, height, heater inlet temperature, pressure and local loss coefficients and stability behavior of a Supercritical Water Natural Circulation Loop (SCWNCL) were studied. It was found that the larger diameter loops are more unstable in terms of heater power compared to small diameter loops for supercritical water natural circulation, however smaller diameter loops are unstable over a wide range of heater outlet temperature for a fixed heater inlet temperature. Liu et al. (2014) investigated the stability characteristics of parallel-channel systems based on linear stability analysis using frequency-domain model. The prototype of their systems used is originated from the thermal-spectrum zone assemblies of a newly designed mixed-spectrum SCWR (SCWR-M). Marginal stability boundaries MSBs under several conditions were obtained, which indicate that the system normal operational condition is in an absolute stable region. Their results also indicate that decreasing the wall thermal conductivity can improve system stability while increasing mass flow is beneficial for the system stability. The system is not very sensitive to the axial power distributions. They also developed one-dimensional time-domain model for nonlinear analysis of the system. The MSBs obtained using the time-domain model were in good agreement with that of frequency-domain model. They came to conclusion that the second eigenvalue should be considered when studying the stability characteristics of complicated systems by using frequency-domain methods. Natural convective flow and heat transfer studies for supercritical water in a rectangular circulation loop were performed by Sharma et al. (2014). Instability was observed over a narrow window of power in the pseudo-critical temperature region. Instability was also observed at low supercritical pressure range of 22.1–22.9 MPa, however it got suppressed at higher pressures.

Xi et al. (2014b) carried out a three dimensional (3D) numerical simulation using CFX code to investigate the out of phase oscillation between two heated parallel channels with supercritical water. Results show that the 3D code predicted the onset of flow instability better than 1D code, but could not quite well predict the period of oscillation. Xi et al. (2014a) and Xiong et al. (2012) performed experiment studies which concerned with out of phase flow instability between two heated parallel channels with supercritical water. Xi et al. analyzed dynamics characteristics of out of phase oscillation and obtained instability boundaries under different inlet temperatures, axial power shapes, total inlet mass flow rates and system pressures. They indicate that system will be more stable with a uniform axial power shape, and more stable at low inlet temperatures. Their results also show that with the increase of total inlet mass flow rate, system will become more unstable at higher power boundaries. They described instability boundaries using non-dimensionless parameters, inlet temperature and ratio of critical or threshold power to mass flow rate. Xiong et al. disregarded shot-life transient oscillations and considered only the sustained out-of-phase oscillations accompanied by evident amplitude during the experiment. Their parametric studies show that the flow becomes more stable with increasing pressure or decreasing inlet temperature. Their discussions indicate that the asymmetry of flow rate between parallel channels will be enlarged with relatively higher fluid temperature or total mass flow rate, and making the occurrence of parallel flow instability more difficult in experiments. They finally obtained stability boundaries in a two-dimensional plane using two different approaches: two ID dimensionless parameters proposed for supercritical flow, and non-dimensionless parameters such as inlet temperature and threshold heat flux. Dutta et al. (2015a,b) investigated the parallel channel density wave instability in the CANDU supercritical water reactor (SCWR) using a 1-D thermal-hydraulic model, THRUST, in the time domain. The in-phase and out-of-phase modes of density wave oscillations DWOs investigated were originated from instabilities purely due to the thermal-hydraulic feedbacks, the influence of neutronic reactivity feedback effects was not taken into consideration. Marginal stability boundaries MSBs for both in-phase and out-of-phase modes of DWOs in the CANDU SCWR were obtained based on 1-D dimensionless numbers. The effect of various parameters, such as mass flow rate, operating pressure, axial heat flux profile, local pressure drop coefficient, and friction factor on the stability thresholds of the reactor have been investigated. Zhang et al. (2016) investigated DWOs experimentally at supercritical pressures in two parallel channels with supercritical water. Based on stability map drawn using Ambrosini's non-dimensional parameters (Ambrosini and Sharabi, 2008), it was indicated that no instability occurs when the exit fluid temperature is below the pseudo-critical temperature regardless of the system pressure, inlet temperature, heating power, and local loss coefficient. For identification purposes especially during experiments, often it becomes necessary to quantify the amplitude of oscillations as a certain percentage of the steady state value. Amplitudes more than ±10% of the mean value is often considered as an indication of instability. However, some authors recommend the use of ±30% as the cutoff value (Ampomah-Amoako, 2013; Nayak and Vijayan, 2008).

The type of axial power distribution adopted in supplying heat to fluid flowing through heat transfer systems has significant effect on heat transfer and flow instability at supercritical pressures (Xi et al., 2014a). This study employed 3D numerical code STAR-CCM +CFD code to investigate the effects of axially decreased and homogeneous axial power distributions on supercritical flow instability in parallel channels.

2. Reference experimental setup and adopted 3D geometry

The geometry adopted in this work is the experimental geometry by Xi et al. (2014a) with focus on the fluid region. A flow instability experiment between two heated channels with supercritical water was carried out by Xi in Nuclear Power Institute of China (NPIC) (Xi et al., 2014a). Supercritical flow instability had been investigated in the experiment under different system pressures,

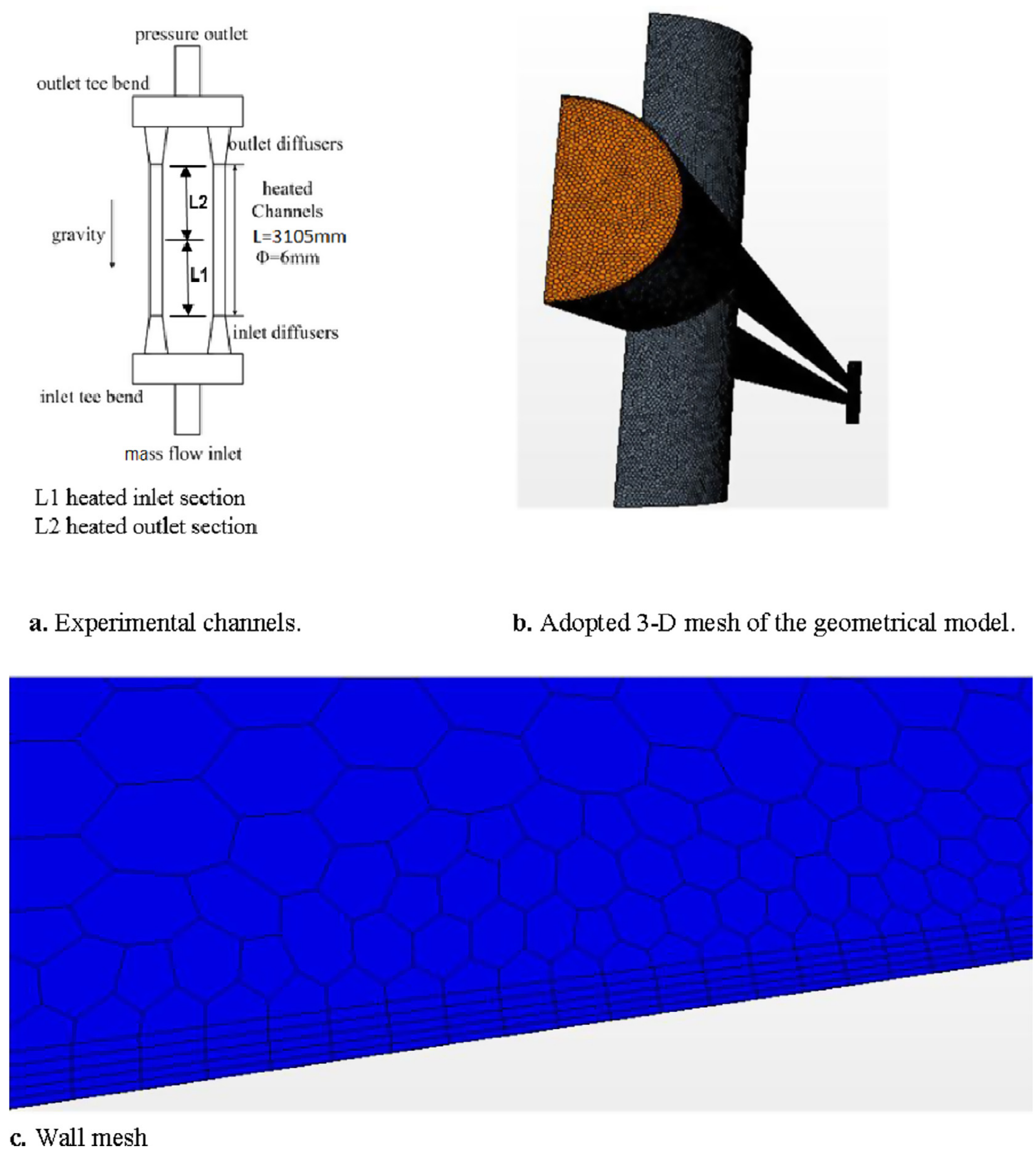

Fig. 5. Schematic diagram of the experimental channels (a), 3-D mesh (b), and Wall mesh (c) in the numerical simulation.

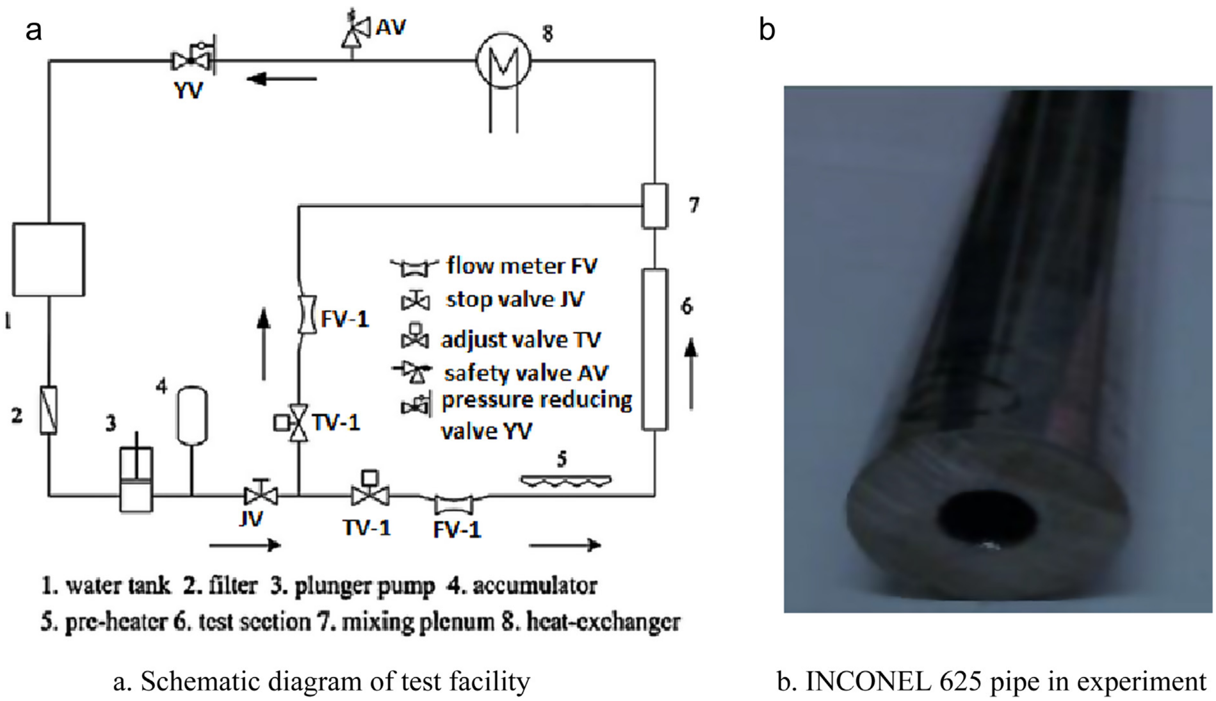

Fig. 6. The schematic diagram of test facility and INCONEL 625 pipe in experiment.

inlet mass flow rates, inlet temperatures and axial power shapes. The test section of the geometrical model consists of two parallel channels with inner diameter 6 mm, outer diameter 19 mm and heated length of 3105 mm as shown in Fig. 5a. The adopted STAR-CCM+3-D mesh of the geometrical model and the Wall mesh are also shown respectively in Fig. 5b and c. The schematic diagram of experimental test facility used in operating the parallel channels is shown in Fig. 6a. The INCONEL 625 pipe in experiment used for the parallel channels in the test section is also shown in Fig. 6b. The total mesh size with 1.0 mm base size of the two tee bends, four diffusers and 2 heated parallel channels is approximately 2785000. Polyhedral Mesher, Prism Layer Mesher and Surface Remesher were selected for the meshing. Half of the full geometry (symmetrical boundary condition) was used in order to save computational time. Non-Slip wall boundary condition was adopted at the wall. Adiabatic boundary condition was adopted for the non-heated walls and heat flux boundary condition was adopted for the heated walls of the parallel channel. Mass flow rate inlet and pressure outlet boundary conditions were adopted for the inlet and outlet respectively. The design and operating pressures are respectively 30 MPa and 25 MPa, and design and operating temperatures are respectively 550 °C and 500 °C. The heating powers applied in the experiment are net heating powers applied to the fluid region in the test section of the experimental set-up. The heat loss had been taken care off in the experiment. The numerical simulation considered only the fluid region and the net heating powers were applied to the fluid region too for the numerical simulations. The focus of the study is not on effects of heating structures where the thickness of the pipe has to be taken into consideration in the geometrical modelling. Greater detail about the experimental facility and the experiment is reported in Xi et al. (2014a).

To ensure that the inlet and outlet pressure loss coefficients employed in the experiment and numerical simulation are the same, the pressure jump model was used in the numerical simulation to adjust the inlet and outlet pressure loss coefficients. The inlet and outlet pressure loss coefficient used in the experiment are:

K_{in1} = 4.1, K_{in2} = 4.3; and K_{out1} = 3.9, K_{out2} = 3.8.

3. Physical models

Mass conservation equation:

$$\frac{\partial \rho}{\partial t} + \nabla.(\rho\vec{u}) = 0 \tag{1}$$

U- Momentum equation:

$$\frac{\partial(\rho u)}{\partial t} + div(\rho u\vec{u}) = div(ugradu) - \frac{\partial P}{\partial x} + \left[-\frac{\partial(\rho\overline{u'^2})}{\partial x} - \frac{\partial(\rho\overline{u'v'})}{\partial y} - \frac{\partial(\rho\overline{u'w'})}{\partial z}\right] + S_u, (2) \tag{2}$$

V- Momentum equation:

$$\frac{\partial(\rho v)}{\partial t} + div(\rho v\vec{u}) = div(ugradv) - \frac{\partial P}{\partial y} + \left[-\frac{\partial(\rho\overline{u'v'})}{\partial x} - \frac{\partial(\rho\overline{v'^2})}{\partial y} - \frac{\partial(\rho\overline{v'w'})}{\partial z}\right] + S_v \tag{3}$$

W- Momentum equation:

$$\frac{\partial(\rho w)}{\partial t} + div(\rho w\vec{u}) = div(ugradw) - \frac{\partial P}{\partial x} + \left[-\frac{\partial(\rho\overline{u'w'})}{\partial x} - \frac{\partial(\rho\overline{w'v'})}{\partial y} - \frac{\partial(\rho\overline{w'^2})}{\partial z}\right] + S_w \tag{4}$$

Energy conservation equation:

$$\frac{\partial(\rho T)}{\partial t} + div(\rho\vec{u}T) = div\left(\frac{\lambda}{C_p}gradT\right) + \left[-\frac{\partial(\rho\overline{u'T'})}{\partial x} - \frac{\partial(\rho\overline{v'T'})}{\partial y} - \frac{\partial(\rho\overline{w'T'})}{\partial z}\right] + S_T \tag{5}$$

where the symbols have their usual meanings (Xi et al., 2014b; Versteeg and Malalasekera, 1995).

Three 3 different turbulence models were tested for their ability to capture the experimentally observed instability. These turbulence models include realizable k-ε model, standard k–ε model and k-ω SST model (Cd-Adapco, 2015) with a high- y^+ wall treatment.

The turbulence kinetic energy and dissipation rate equations to be solved in realizable k-ε model are as follows:

$$\frac{\partial(\rho k)}{\partial t}+\frac{\partial(\rho k u_i)}{\partial x_j}=\frac{\partial}{\partial x_j}\left[\left(\mu+\frac{\mu_t}{\delta_k}\right)\frac{\partial k}{\partial x_j}\right]+G_k+G_b-\rho\varepsilon-Y_M+S_k \tag{6}$$

$$\frac{\partial(\rho\varepsilon)}{\partial t}+\frac{\partial(\rho\varepsilon u_i)}{\partial x_j}=\frac{\partial}{\partial x_j}\left[\left(\mu+\frac{\mu_t}{\delta_\varepsilon}\right)\frac{\partial\varepsilon}{\partial x_j}\right]+\rho C_1 S\varepsilon-\rho C_2\frac{\varepsilon^2}{k+\sqrt{\nu\varepsilon}}+C_{1\varepsilon}\frac{\varepsilon}{k}C_{3\varepsilon}G_b+S_\varepsilon, \tag{7}$$

The turbulence kinetic energy and dissipation rate equations to be solved in standard k-ε model are:

$$\frac{\partial(\rho k)}{\partial t}+\frac{\partial(\rho k u_i)}{\partial x_j}=\frac{\partial}{\partial x_j}\left[\left(\mu+\frac{\mu_t}{\delta_k}\right)\frac{\partial k}{\partial x_j}\right]+G_k+G_b-\rho\varepsilon-Y_M+S_k \tag{8}$$

$$\frac{\partial(\rho\varepsilon)}{\partial t}+\frac{\partial(\rho\varepsilon u_i)}{\partial x_j}=\frac{\partial}{\partial x_j}\left[\left(\mu+\frac{\mu_t}{\delta_\varepsilon}\right)\frac{\partial\varepsilon}{\partial x_j}\right]+C_{1\varepsilon}\frac{\varepsilon}{k}(G_k+C_{3\varepsilon}G_b)-C_{2\varepsilon}\rho\frac{\varepsilon^2}{k}+S_\varepsilon \tag{9}$$

The turbulence kinetic energy and specific dissipation rate equations to be solved in k-ω SST model are described as:

$$\frac{\partial(\rho k)}{\partial t}+\frac{\partial(\rho k u_i)}{\partial x_j}=\frac{\partial}{\partial x_j}\left[\left(\mu+\frac{\mu_t}{\delta_k}\right)\frac{\partial k}{\partial x_j}\right]+G_k+G_b-Y_k+S_k \tag{10}$$

$$\frac{\partial(\rho\omega)}{\partial t}+\frac{\partial(\rho\omega u_i)}{\partial x_j}=\frac{\partial}{\partial x_j}\left[\left(\mu+\frac{\mu_t}{\delta_\omega}\right)\frac{\partial\omega}{\partial x_j}\right]+G_\omega+D_w-Y_\omega+S_\omega(11) \tag{11}$$

$$\sigma_k=1;\ \sigma_\varepsilon=1.2;\ C_{1\varepsilon}=1.44;\ C_2=1.9;\ C_{3\varepsilon}=\tan\left|\frac{w_{//\vec{g}}}{w_{\perp\vec{g}}}\right| \tag{12}$$

$$C_1=\max\left[0.43,\frac{\eta}{\eta+5}\right];\ \eta=S\frac{k}{\varepsilon};\ S=\sqrt{2S_{ij}S_{ij}} \tag{13}$$

As in many other available CFD codes, STAR-CCM+ makes use of finite volume discretization technique to discretize the equations. The method of discretization is beyond the scope of the work.

4. Results

4.1. Time step and turbulence model considerations

In this work, the coolant inlet temperature and the ratio of heating power (threshold or critical power) to inlet mass flow rate are adopted to obtain the instability boundary for 3D analysis, a method already used by Xi et al. (2014a,b).

In order to obtain the instability boundary, the total inlet mass flow rate is kept constant at a particular pressure, the inlet mass flow rates M_{in1} and M_{in2} are monitored for the occurrence of out of phase flow oscillation at a particular heating power. The stabilization of the average surface temperatures of the outlets of channels 1 and 2 is used to determine the convergence of the simulation, different from the residual method adopted by Xi to determine the convergence (Xi et al., 2014b). The numerical simulations performed by Xi were compared with experimental results in Xiong et al. (2012). The outlet temperature starts to rise steadily as the fluid is heated in the channels. The stabilization of the surface average outlet temperature of the heated section is adopted for convergence because the residual values begin to increase as flow oscillation starts to develop. "The stabilization of the average surface temperatures of the outlets of the heated channels 1 and 2" referred to means that the outlet temperature in each channel fluctuates around particular maximum outlet temperature with no more steady increase in the outlet temperature at the point of convergence. The residual values stabilize as the flow oscillations are fully developed. If out of phase flow oscillation is not observed in M_{in1} and M_{in2}, the heating power is increased and the two inlet mass flow rates are observed again for the occurrence of out of phase flow oscillation. This process is repeated until there is out of phase flow oscillation in M_{in1} and M_{in2} with amplitude greater than 5%, the heat flux is recorded and the equivalent power called Threshold or Critical power is calculated. Any heating power above the Critical power will make the system unstable otherwise it will be stable. The occurrence of out of phase flow oscillation is observed in M_{in1} and M_{in2} for various coolant inlet temperatures in this way and the corresponding Critical powers are used for plotting the instability boundary curve. The coolant inlet temperature ranges from 180 °C to 320 °C, and heating powers used for the various numerical simulations are in the range of 67 kW to 120 kW. NIST table (NIST, 2002) was used to generate the physical properties of water.

In 3D numerical simulation, the type of models used for simulation will affect the precision of calculation (Xi et al., 2014b). These models include mesh number, solution technique (velocity-pressure coupling method, or segregated flow approach), time step, difference scheme, turbulence model, etc. Also, it is noted that the type of power shape adopted for performing experimental research will affect the experimental results (Xi et al., 2014a). In this work, the time step and turbulence model were first analyzed and the suitable models were adopted for various simulations. Implicit formulation was adopted, the governing equations were solved using segregated flow approach and effect of gravity was taken into consideration in all the numerical simulations.

Figs. 7–10 respectively show numerical simulation results obtained for four time steps, 0.005 s, 0.01 s, 0.02 s, and 0.03 s tested in this work. Operating conditions include 23 MPa system pressure, mass flow rate of 125 kg/h and 260 °C inlet temperature. Axially decreased power shape was adopted. For a total heating power of 85.0 kW, 21.25 kW was applied to the heating wall of the heated inlet section for 30 s; 3.54 kW, 7.08 kW and 10.63 kW were applied to the heating wall of the heated outlet section for 10 s respectively. These system parameter values for axially decreased power shape are summarized in Table 1. Both the inlet and outlet heated sections were heated for equal time duration of 30 s, hence the choice of 10 s time interval for the axially decreasing power shape for each power step for the heated outlet

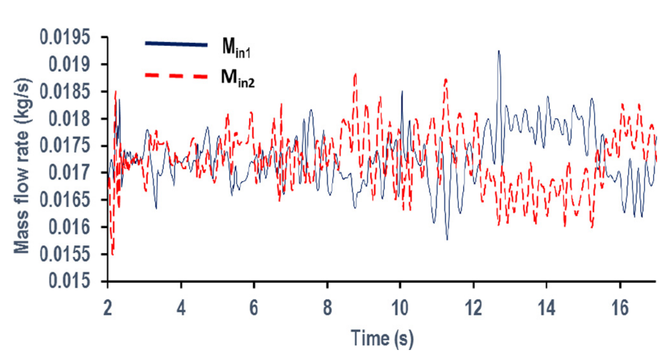

Fig. 7a. Inlet mass flow rate oscillation of each channel, 0.005 s.

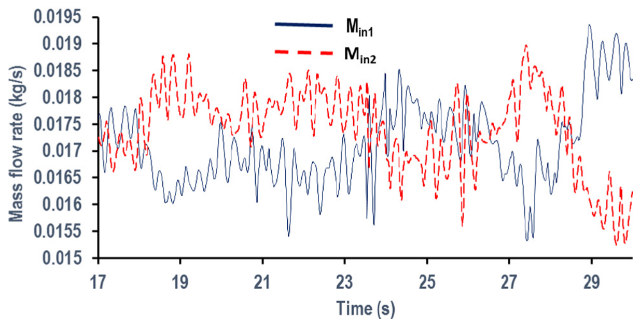

Fig. 7b. Inlet mass flow rate oscillation of each channel, 0.005 s.

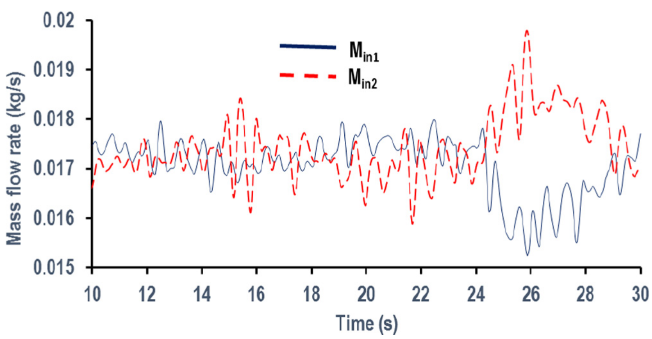

Fig. 8. Inlet mass flow rate oscillation of each channel, 0.01 s.

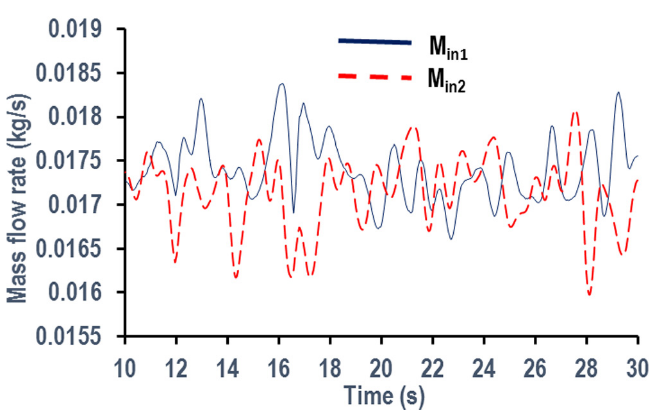

Fig. 9. Inlet mass flow rate oscillation of each channel, 0.02 s.

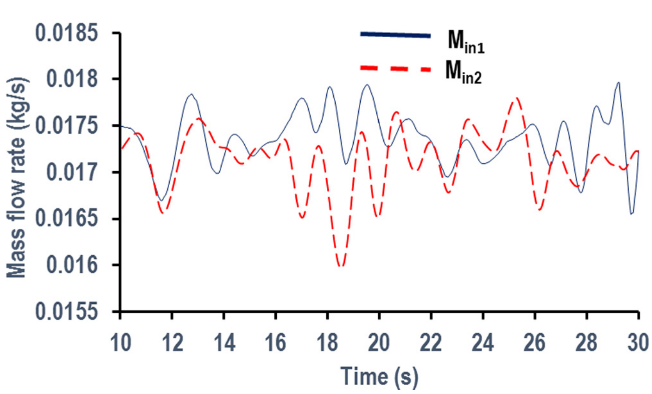

Fig. 10. Inlet mass flow rate oscillation of each channel, 0.03 s.

section. Results for maximum inlet mass flow oscillation amplitude and period of oscillations for each time step are shown in Table 2.

The time step of 0.005 s could capture the dynamic characteristics of the flow very well compared to the other time steps. The results also show that time step has significant effect on flow instability, and the dynamic characteristics of the flow might not be captured well if reasonable and optimum smaller time step was not used for the numerical simulation. Generally, the unsteady 3D simulation is time consuming especially when time step is short. Time step of 0.01 s was used for the numerical simulations. From the trend of the results, much smaller time step could capture the dynamics characteristics much better but would be computationally too much expensive for this work.

Figs. 11–13 respectively show results for three turbulence models, standard k–ε model; realizable k-ε model; and k-ω SST model examined in this work. The simulations were carried out at coolant inlet temperature of 250 °C, mass flow rate of 125 kg/h and 23 MPa system pressure. Axially decreased power shape was adopted. For a total heating power of 120.0 kW, 30 kW was applied to the heating wall of each inlet heated section for 30 s; and 5 kW, 10 kW and 15 kW were applied to the heating wall of each outlet heated section for 10 s respectively. These system parameter values for axially decreased power shape are summarized in Table 3. The maximum amplitudes and periods of out of phase inlet mass flow oscillations of the respective three turbulence models are 40 kg/h and 1.0 s; 13 kg/h and 0.9 s; and 8 kg/h and 0.9 s. The results of these simulations are shown in Table 4. The results show that the three turbulence models tested predicted approximately the same period of mass flow oscillation but predicted different amplitudes of mass flow oscillations, indicating that the appropriate choice of turbulence model for the numerical simulation is important for the numerical tool adopted to capture quite well the dynamics characteristics of the flow. The largest amplitude of 40 kg/h was predicted by the standard k-Epsilon turbulence model and hence could predict flow instability quite well than the Realizable k-Epsilon and k-ω SST turbulence models. The standard k-Epsilon turbulence model was adopted for the numerical simulations.

4.2. Influence of axial power shape

Axially decreased and homogeneous axial power shapes were considered in this work. The heated section was divided into inlet and outlet heated sections for Axially Decreased Power Shape ADPS. For ADPS, the heat flux applied to the heating wall of the inlet heated section is more than the heat flux applied to the heating wall of the outlet heated section, and for Homogeneous Axial Power Shape HAPS constant heat flux is applied to the heated section. Two mass flow rates 125 kg/h and 145 kg/h were used for the numerical simulations. For ADPS, 20.75 kW was applied to the heating wall of each heated inlet section for 125 kg/h, and 24.0 kW was applied to the heating wall of each heated inlet section for 145 kg/h (Xi et al., 2014a). The heated section was divided into inlet and outlet heated sections for ADPS.

Fig. 14 shows the instability boundaries for axially decreased and homogeneous axial power shapes for inlet temperatures varying from 180 °C to 320 °C, system pressure of 23 MPa, total mass flow rate of 125 kg/h and with the influence of gravity. The stability of a system with each of the two power shapes decreases with increase of inlet temperature up to inflection point at (67.2 kW, 240 °C) for axially decreased power shape (ADPS) and at (71.2 kW, 240 °C) for homogeneous axial power shape (HAPS) and increases thereafter. Jingjing et al. (2015) reported similar findings for HAPS. The system with HAPS is more stable than that of ADPS for all the inlet temperatures, a similar finding was also reported by Xi et al. (2014a).

Table 1
System parameter values for axially decreased power shape (time step).

Parameters	Value	Heating power and time of heat application			
		Each inlet heated section		Each outlet heated section	
		Power, kW	Time, s	Power, kW	Time, s
Pressure, MPa	23				
Mass flow rate, kg/h	125				
Inlet temperature, °C	260	21.25	30.0	3.54	10.0
				7.08	10.0
				10.63	10.0

Table 2
Amplitudes and periods of oscillations for various time steps.

Time step, s	Amplitude, kg/h	Period, s
0.005	10.8	0.5
0.01	7.8	1.0
0.02	6.5	1.6
0.03	4.8	1.8

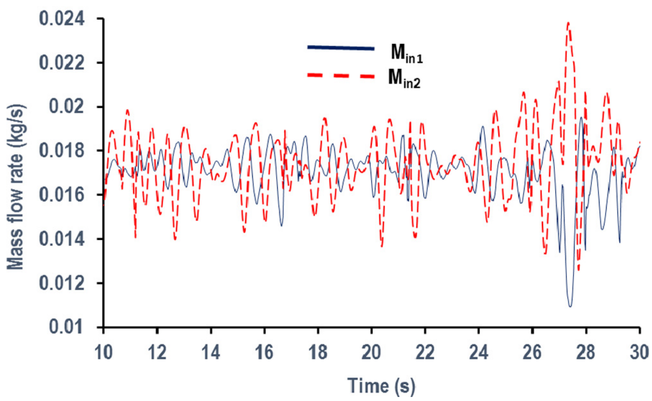

Fig. 11. Inlet mass flow rate oscillation of each channel, Standard k–ε model.

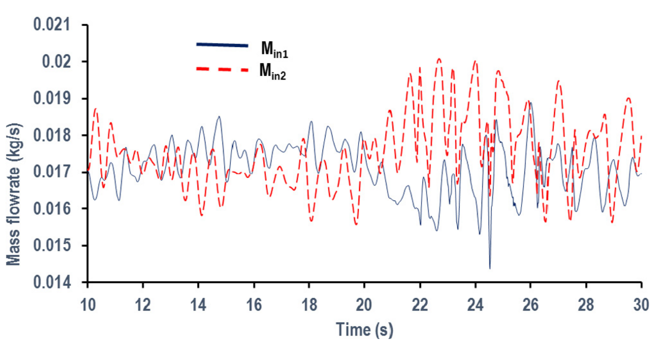

Fig. 12. Inlet mass flow rate oscillation of each channel, Realizable k-ε model.

4.3. Influence of axial power shape on system pressure

Fig. 15 shows the instability boundaries for axially decreased and homogeneous axial power shapes for system pressure of 25 MPa, mass flow rate of 125 kg/h and with gravity influence. With the increase of the system pressure from 23 MPa (Fig. 14) to 25 MPa, the stability of each of the two power shapes increases but the increment associated with HAPS is more than that of ADPS. The inflection point for ADPS is (68.0 kW, 240 °C) and that of HAPS is (77.2 kW, 260 °C). For the two system pressures, the stability decreases and increases respectively below and above a corresponding inflection point with the increase of inlet temperature. The system is more stable with HAPS at both system pressures of 23 MPa and 25 MPa.

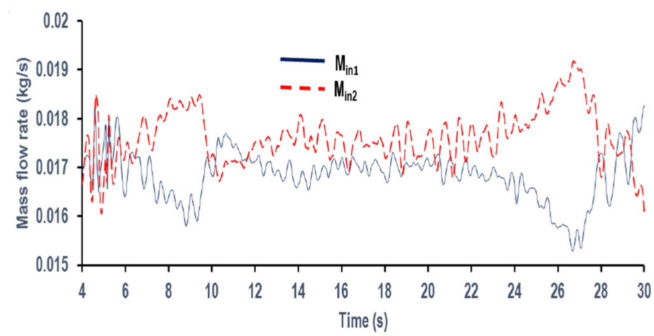

Fig. 13. Inlet mass flow rate oscillation of each channel, k-ω SST model.

4.4. Influence of axial power shape on mass flow rate

Fig. 16 shows the instability boundaries for axially decreased and homogeneous axial power shapes for system mass flow rate of 145 kg/h, system pressure of 23 MPa and with gravity influence. With the increase of system mass flow rate from 125 kg/h (Fig. 14) to 145 kg/h, the stability of ADPS decreases with inlet temperature with no inflection point whereas the stability of the HAPS decreases and increases respectively below and above the inflection point of (81.2 kW, 240 °C) with increasing inlet temperature. At low inlet temperatures, the system is more stable with ADPS but at high inlet temperatures, the system is more stable with HAPS for the system operated at 145 kg/h, 23 MPa and with gravity influence. With the increase of the system mass flow rate to 145 kg/h, the system with ADPS becomes more stable at low inlet temperatures and less stable at high inlet temperatures, whereas the system with HAPS becomes less stable for various inlet temperatures. Su et al. (2013), Xiong et al. (2013), Liu et al. (2014) and Jingjing et al. (2015) obtained similar finding that stability of a system increases with growing of the system mass flow rate. But Xi et al. (2014a,b) obtained the finding that stability of a system decreases with increasing growing of the system mass flow rate, which is in agreement with the obtained numerical results for HAPS in this work.

4.5. Influence of axial power shape on gravity

Fig. 17 shows the instability boundaries for axially decreased and homogeneous axial power shapes for a system with pressure of 23 MPa, mass flow rate of 125 kg/h and without the influence of gravity. The system with ADPS or HAPS becomes more stable with the change of the system with the influence of gravity (Fig. 14) to the system without the influence of gravity. The stability increment associated with the system with HAPS is more than that of the system with ADPS for the system without gravity influence. For the system without the influence of gravity, the stability decreases and increases respectively below and above the inflection point of (68.5 kW, 260 °C) for ADPS and (80.6 kW, 280 °C) for HAPS with inlet temperature (Fig. 17). This explains why, depending on the other operating parameters, the horizontally

Table 3
System parameter values for axially decreased power shape (turbulence model).

Parameters	Value	Heating power and time of heat application			
Pressure, MPa	23	Each inlet heated section		Each outlet heated section	
Mass flow rate, kg/h	125	Power, kW	Time, s	Power, kW	Time, s
Inlet temperature, °C	250	30.0	30.0	5.0 10.0 15.0	10.0 10.0 10.0

Table 4
Amplitudes and periods of oscillations for various turbulence models.

Turbulence model	Amplitude, kg/h	Periods, s
Standard k-Epsilon	40	1.0
Realizable k-Epsilon	13	0.9
k-ω SST	8	0.9

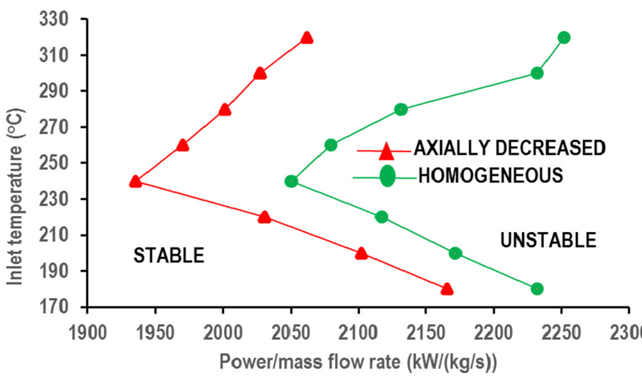

Fig. 14. Influence of axial power shape (P = 23 MPa, M_t = 125 kg/h, with gravity).

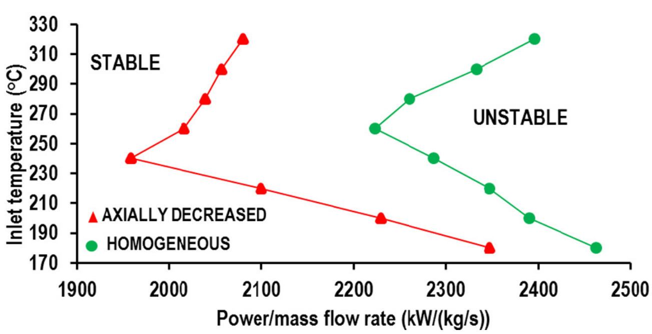

Fig. 15. Influence of axial power shape on system pressure (P = 25 MPa).

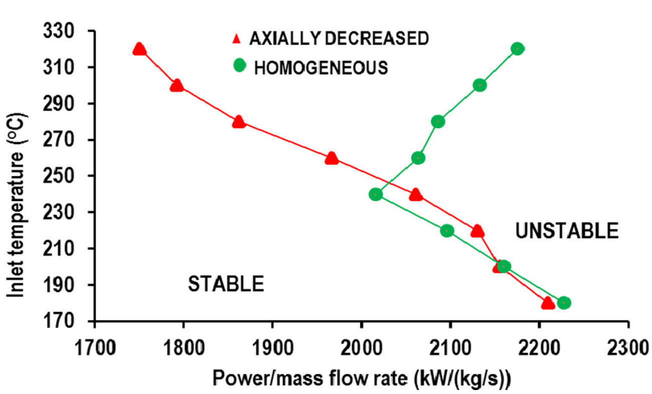

Fig. 16. Influence of axial power shape on system mass flow rate (M_t = 145 kg/h).

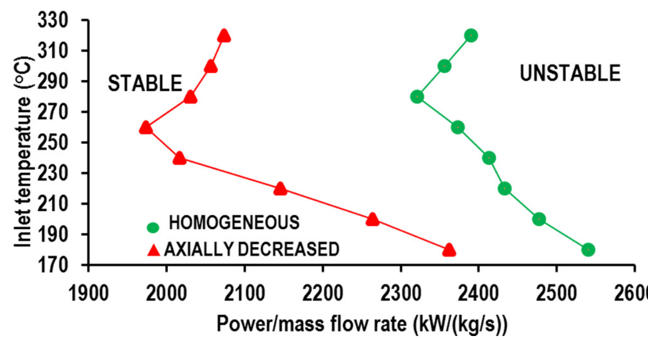

Fig. 17. Influence of axial power shape on gravity (without gravity).

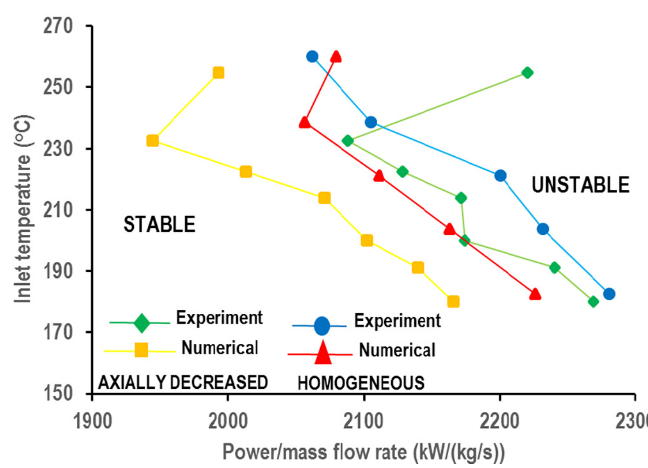

Fig. 18. Comparison between Numerical and Experimental results, Instability boundaries (axially decreased and homogeneous axial power distributions).

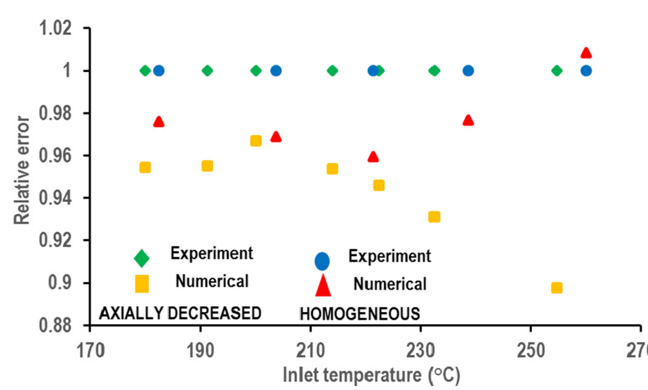

Fig. 19. Comparison between Numerical and Experimental results (axially decreased and homogeneous axial power distributions).

Table 5
Numerical threshold power compared with Experimental threshold power.

Homogeneous axial power distribution			Axially decreased power distribution		
Inlet temperature °C	Experimental threshold power, kW	Numerical threshold power, kW	Inlet temperature °C	Experimental threshold power, kW	Numerical threshold power, kW
182.5	79.2	77.3	180.0	78.8	75.2
203.8	77.5	75.1	191.3	77.8	74.3
221.3	76.4	73.3	200.1	75.5	73.0
238.7	73.1	71.4	214.0	75.4	71.9
260.0	71.6	72.2	222.4	73.9	69.9
			232.5	72.5	67.5
			254.8	77.1	69.2

oriented reactor type such as CANDU-SCWR type may be more stable to operate than the vertically oriented reactor types such as Japan, Europe, Korea and USA SCWRs. The system with HAPS is more stable than that with ADPS when operated with or without gravity influence.

4.6. Comparison of numerical results with experimental results

Fig. 18 shows numerical and experimental instability boundaries for axially decreased and homogeneous axial power shapes at system mass flow rate of 125 kg/h, pressure of 23 MPa, inlet temperatures from 180 °C to 260 °C and with gravity influence. For ADPS, there is inflection point (67.5 kW, 232.5 °C) for numerical and (72.5 kW, 232.5 °C) for experimental, below which stability decreases and above which stability increases with inlet temperature. For HAPS, there is inflection point (71.4 kW, 238.7 °C) below which stability decreases and above which stability increases with inlet temperature for the numerical results, but there is no inflection point for experimental results and the stability decreases with inlet temperature. Both the numerical and experimental homogeneous axial power shapes are more stable than the corresponding numerical and experimental axially decreased power shapes. Fig. 19 and Table 5 quantitatively compare the numerical and experimental results of ADPS and HAPS at operating conditions of 23 MPa, 125 kg/h and with gravity influence, and almost all the numerical results are within the acceptable error limit of ± 10%. But the 3D numerical tool adopted mostly under-predicted the experimental results for both axial power shapes.

Figs. 20 and 21 show numerical and experimental inlet mass flow oscillations at 23 MPa, 125 kg/h, 192 °C and with gravity influence for ADPS with a heating power of 81.5 kW. For the total heating power of 81.5 kW, 20.75 kW was applied to the heating wall of each inlet heated section for 78 s; and 4.71 kW, 6.66 kW and 8.62 kW were applied to the heating wall of each outlet heated section for 26 s respectively. These system parameter values for axially decreased power shape are summarized in Table 6. Maximum amplitudes of 7.2 kg/h and 25 kg/h were obtained for numerical and experimental results; and periods of 1.0 s and 1.3 s were obtained for numerical and experimental results respectively.

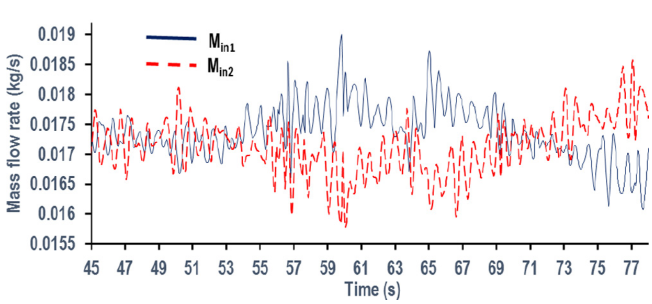

Fig. 20. Inlet mass flow rate oscillation of each channel (numerical).

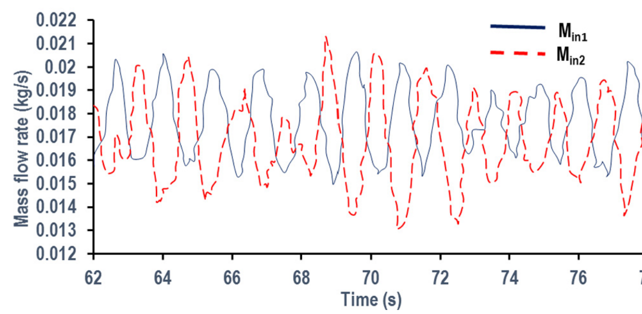

Fig. 21. Inlet mass flow rate oscillation of each channel (experiment).

Table 6
System parameter values for axially decreased power shape.

Parameters	Value	Heating power and time of heat application			
Pressure, MPa	23	Each inlet heated section		Each outlet heated section	
Mass flow rate, kg/h	125	Power, kW	Time, s	Power, kW	Time, s
Inlet temperature, °C	192	20.75	78.0	4.71 6.66 8.62	26.0 26.0 26.0

The numerical tool adopted largely under-predicted experimental amplitude and quite well predicted experimental period of the inlet mass flow oscillations. The differences in the numerical amplitude and period of the oscillations compared to that of the experiments might be due to the use of larger time step because of computational time cost, and also the inability of the turbulence model adopted to accurately capture the experimental amplitude and period of the oscillations.

5. Conclusions

This work investigates effect of axial power distribution on flow instability in parallel channels with water at supercritical pressures. The axial power distribution considered include axially decreased and homogeneous axial power shapes. The study also seeks to examine the performance of the numerical tool STAR-CCM+ in predicting instability boundaries at supercritical pressures. The parameters such as mass flow rate, pressure and gravity are considered in the investigation. The following findings are obtained during the investigation:

- The stability of a system with each of the two axial shapes, axially decreased and homogeneous, decreases and increases respectively below and above different threshold power with inlet temperature but the system is more stable with HAPS than that of ADPS for a system operated at two different pressures 23 MPa and 25 MPa, mass flow rate of 125 kg/h, inlet temperatures from 180 °C to 320 °C and with gravity influence. Similar observation was made for a system operated at mass flow rate of 125 kg/h, system pressure of 23 MPa, and with or without gravity influence. For a system operated at 145 kg/h, 23 MPa and with gravity influence, there is a threshold power below which stability decreases and above which stability increases with inlet temperature for HAPS, but there is no inflection point for ADPS and the stability deceases with inlet temperature. At low inlet temperatures, the system is more stable with ADPS but at high inlet temperatures, the system is more stable with HAPS for the system operated at 145 kg/h and 23 MPa.

- The system with ADPS or HAPS becomes more stable with the change of the system operated with gravity influence to system operated without gravity influence, and also with the change of system pressure from 23 MPa to 25 MPa. With the change of the system mass flow rate from 125 kg/h to 145 kg/h, the system with ADPS becomes more stable at low inlet temperatures and less stable at high inlet temperatures, whereas the system with HAPS becomes less stable for various inlet temperatures.
- For a system with ADPS or HAPS and operated under experimental conditions of 125 kg/h mass flow rate, 23 MPa pressure, inlet temperatures from 180 °C to 260 °C and with gravity influence, the trends of the numerical instability boundary results agree quite well with the trends of the experimental instability boundary results for most of the inlet temperatures, but there is no inflection point for experimental HAPS as it is the case for the numerical HAPS. The system with HAPS is more stable than that with ADPS, a finding also obtained for the experimental results.
- The dynamic characteristics such as amplitude and period were also compared with experimental results for ADPS at mass flow rate of 125 kg/h, 23 MPa, and with gravity influence. The experimental amplitude was largely under-predicted and the experimental period was quite well predicted by the numerical tool adopted.
- The results of this study show that the type of axial power shape adopted in supplying heat to the fluid flowing through heat transfer system has significant effect on stability of the system. From the comparison of the numerical and experimental results, the 3D numerical tool, STAR-CCM + code could predict flow instability in the parallel channels irrespective of the type of axial power shape adopted. However, there is an evidence that the presence of heating structures in the geometrical model adopted may change the predicted behavior, as shown in previous works. More relevant experiments at supercritical pressures should be carried out for validation of numerical tools adopted for similar studies.

Acknowledgement

Cd-Adapco is acknowledged for providing a free license and technical support in making this work possible.

References

Ambrosini, W., Sharabi, M.B., 2008. Dimensionless parameters in stability analysis of heated channels with fluids at supercritical pressures. Nucl. Eng. Des. 238, 1917–1929.

Ampomah-Amoako, E., 2013. Stability and Control of SCWR Systems: A Study into Concepts and Applications. PhD thesis submitted to the Department of Nuclear Engineering, Graduate School of Nuclear and Allied Sciences, University of Ghana, Legon.

Dutta, G., Doshi, J.B., 2008. A characteristics-based implicit finite-difference scheme for the analysis of instability in water cooled reactors. Nucl. Eng. Technol. 40 (6).

Cd-Adapco, 2015, User Guide, STAR-CCM+ Version 10.06.009.

Chatoorgoon, V., 2008. Supercritical flow stability in horizontal channels. Nucl. Eng. Des. 238, 1940–1946.

Dutta, G., Zhang, C., Jiang, J., 2015a. Analysis of parallel channel instabilities in the CANDU supercritical water reactor. Ann. Nucl. Energy 83, 264–273.

Dutta, G., Zhang, C., Jiang, J., 2015b. Analysis of flow induced density wave oscillations in the CANDU supercritical water reactor. Nucl. Eng. Des. 286, 150–162.

Jingjing, L., Tao, Z., Mingqiang, S., Qijun, H., Yanping, H., Zejun, X., 2015. CFD analysis of supercritical water flow instability in parallel channels. Int. J. Heat Mass Transfer 86, 923–929.

Liu, P., Hou, D., Lin, M., Kuang, B., Yang, Y., 2014. Stability analysis of parallel-channel systems under supercritical pressure with heat exchanging. Ann. Nucl. Energy 69, 267–277.

Nayak, A.K., Vijayan, P.K., 2008. Flow Instabilities in Boiling Two-Phase Natural Circulation Systems: A Review, Science and Technology of Nuclear Installations, Volume 2008

NIST, 2002. Reference Fluid Thermodynamic and Transport Properties – REFPROP, Aug. (2002), Lemmon, E.W., McLinden, M.O., Hurber, M.L. (Eds.), NIST Standard Reference Database 23 (Software and Source), V. 7.0, U.S. Department of Commerce.

Sharma, M., Pilkhwal, D.S., Vijayan, P.K., Saha, D., Sinha, R.K., 2010. Steady state and linear stability analysis of a supercritical water natural circulation loop. Nucl. Eng. Des. 240, 588–597.

Sharma, M., Vijayan, P.K., Pilkhwal, D.S., Asako, Y., 2014. Natural convective flow and heat transfer studies for supercritical water in a rectangular circulation loop. Nucl. Eng. Des. 273, 304–320.

Su, Y., Feng, J., Zhao, H., Tian, W., Su, G., Qiu, S., 2013. Theoretical study on the flow instability of supercritical water in the parallel channels. Prog. Nucl. Energy 68, 169–176.

Versteeg, H.K., Malalasekera, W., 1995. An Introduction to Computational Fluid Dynamics: The Finite Volume Method. Longman Scientific & Technical, New York.

Xi, X., Xiao, Z., Yan, X., Li, Y., Huang, Y., 2014a. An experimental investigation of flow instability between two heated parallel channels with supercritical water. Nucl. Eng. Des. 278, 171–181.

Xi, X., Xiao, Z., Yan, X., Xiong, T., Huang, Y., 2014b. Numerical simulation of the flow instability between two heated parallel channels with supercritical water. Ann. Nucl. Energy 64, 57–66.

Xiong, T., Xiao Yan, X., Xiao, Z., Li, Y., Huang, Y., Yu, J., 2012. Experimental study on flow instability in parallel channels with supercritical water. Ann. Nucl. Energy 48, 60–67.

Xiong, T., Yan, X., Huang, S., Yu, J., Huang, Y., 2013. Modeling and analysis of supercritical flow instability in parallel channels. Int. J. Heat Mass Transfer 57, 549–557.

Zhang, L., Cai, B., Weng, Y., Gu, H., Wang, H., Li, H., Chatoorgoon, V., 2016. Experimental investigations on flow characteristics of two parallel channels in a forced circulation loop with supercritical water. Appl. Therm. Eng. 106, 98–108.